LA-UR-16-28129
Approved for public release; distribution is unlimited.

Title:	Summaries of FY16 LANL experimental campaigns at the OMEGA and EP Laser Facilities
Author(s):	Loomis, Eric Nicholas; Merritt, Elizabeth Catherine; Montgomery, David; Kim, Yong Ho; Murphy, Thomas Joseph; Johns, Heather Marie; Kline, John L.; Shah, Rahul C.; Zylstra, Alex; Herrmann, Hans W.; Schmitt, Mark J.; Flippo, Kirk Adler; Rasmus, Alexander Martin
Intended for:	Report
Issued:	2016-10-25

Summaries of FY16 LANL experimental campaigns at the OMEGA and EP Laser Facilities

In FY16, Los Alamos National Laboratory carried out 22 shot days on the OMEGA and OMEGA-EP laser facilities in the areas of High Energy Density (HED) Science and Inertial Confinement Fusion (ICF). In HED our focus areas were on radiation flow, hydrodynamic turbulent mix and burn, warm dense matter equations of state, and coupled Kelvin-Helmholtz (KH)/Richtmyer-Meshkov (RM) instability growth. For ICF our campaigns focused on the Priority Research Directions (PRD) of implosion phase mix and stagnation and burn, specifically as they pertain to Laser Direct Drive (LDD). We also had several focused shot days on transport properties in the kinetic regime. We continue to develop advanced diagnostics such as Neutron Imaging, Gamma Reaction History, and Gas Cherenkov Detectors. Below are a summary of our campaigns, their motivation, and main results from this year.

Shear

The LANL Shear campaign is examining instability growth and its transition to turbulence relevant to mix in ICF capsules using experimental platforms with counter-propagating flows about a shear interface to examine KH instability growth. The platform consists of a directly driven shock-tube target with an internal physics package. The physics package consists of two hemi-cylindrical foams separated by a layer of tracer material with gold plugs on opposing ends of the foams to limit shock propagation from the direct drive to only one end of the foam. This geometry collimates the shocks and sets a region of pressure-balanced shear flow at the center of the shock tube. Measurements of the tracer layer (shear interface) mixing dynamics are used to benchmark the LANL BHR turbulence model. The mixing dynamics are characterized by measuring mix-width of the layer as well as by examining multi-dimensional structure growth along the layer surface.

The FY16 Shear campaign continued an effort to examine instability and model initial condition parameter space by varying the characteristics of the target tracer layer. Both FY16 shot days were part of a three shot day study of instability mode-growth due to single-mode initial conditions, which employed sinusoidal tracer foils of various wavelengths as opposed to the previous flat and roughened foil campaigns. The sinusoids force instability growth by pre-seeding a coherent wavelength. In these experiments we observed early-time (pre-shear) jets and “dust-up” structures, which are points of further study, as well as the persistence of the single-mode structures to late times in the experiment. The finished OMEGA mode growth study also confirms a most unstable mode of $\lambda \approx 100\text{-}150\ \mu m$, as predicted by observations of emergent rollers in our NIF experiment and a naïve application of the simple Rayleigh model.

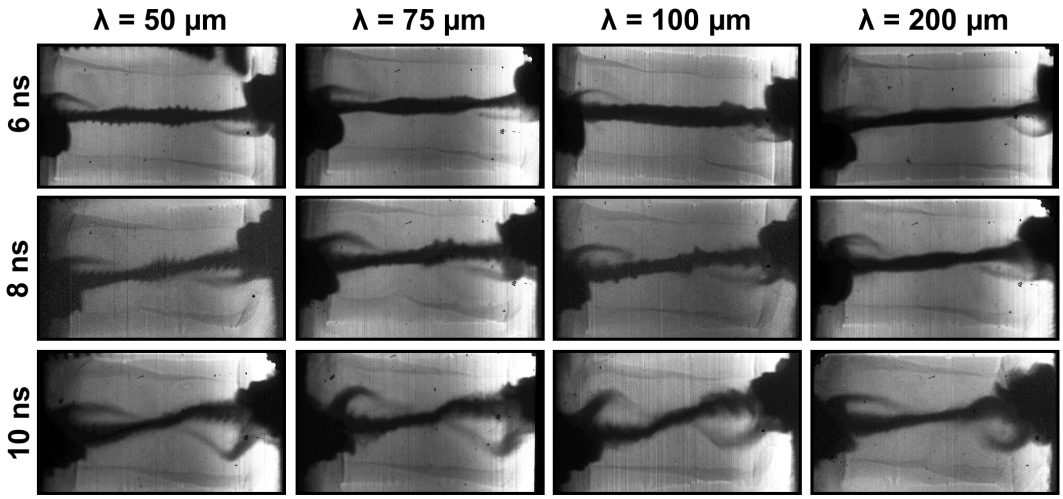

Figure 1: X-ray backlit images of counter-flowing shear experiment showing evolution of foil tracer layer at different perturbation wavelengths

DSPlanar

The LANL DSPlanar OMEGA platform is part of the larger LANL Double Shell campaign. DSPlanar experiments are intended to validate our ability to predict momentum transfer, hydro-coupling and instability growth in a double-shell relevant planar geometry. We choose to use a planar geometry since they are simpler to diagnose than full spherical implosions and can still give us an idea of how well the code simulates fundamental pieces of physics without the added complication of convergence. DSPlanar experiments serve a second purpose as a testing ground for our target fabrication capability development toward NIF Double Shell capsules. DSPlanar target components will use similar materials as NIF Double Shell targets but in a simpler to build geometries. We can use fabrication of these simpler parts as a fist-pass test of our abilities and to identify where we require further R&D resources. The goals of this first DSPlanar shot day were to measure momentum transfer of an ablatively-driven flyer into a mid-Z “inner shell” layer, as well as test NIF relevant ablator materials.

The DSPlanar target is an indirectly driven shock tube with a material stack approximating an unfolded double-shell, with an ablator, a low-density foam cushion, an inner shell surrogate layer, and a final release foam. We varied whether or not we include a tamper layer on the inner shell layer as part of our hydro-instability mitigation studies. The primary diagnostics for the FY16 DSPlanar day were edge-on streaked and imaging radiography. The streaked radiography is designed so we can get measurements of inner shell pre-heat expansion, ablator velocity pre-impact, and system velocity post-impact for momentum transfer studies. On this shot day we identified modifications to the platform required for good streak data and good imaging data. We also obtained comparison data between our standard sample Be ablator targets and AlBeMet (Al/Be alloy) targets required to inform FY17 decisions about our NIF platform.

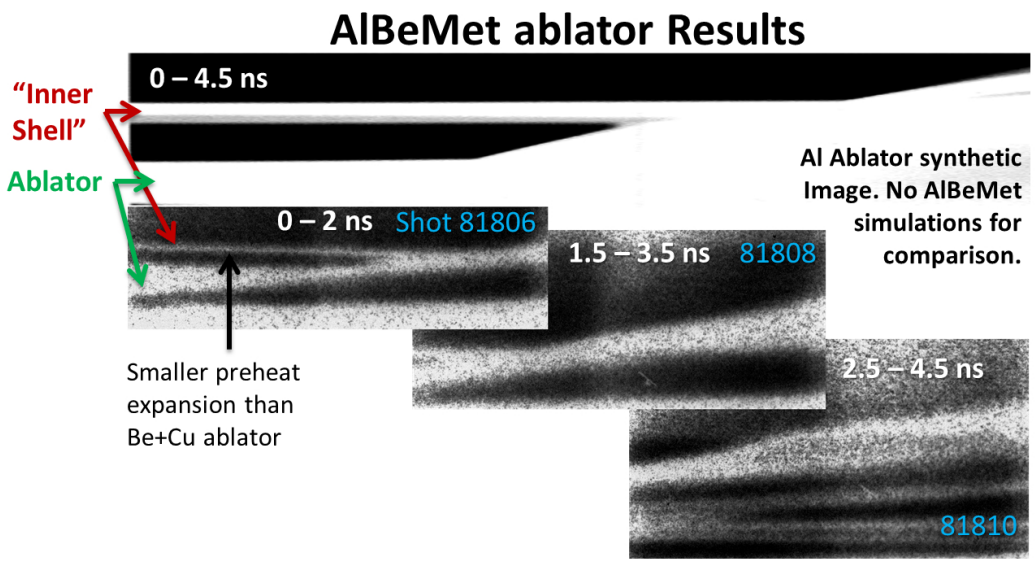

Figure 2: Backlit streak data viewing edge-on of the planar Double Shell experiment

Marble

In the Marble project, nuclear reactants of an ICF implosion are being initially separated via a spherical low-density CD foam matrix infused with a T_2 gas fill. Through advanced target fabrication, voids can be selectively etched into the foam core so as to control the initial separation scale. These cores are encapsulated within a machined ablator and imploded in 60-beam DD with the key measurements being DT and DD yields. In FY 16 experiments at OMEGA, targets have been imploded with both an intrinsic foam structure as well as from foam with engineered voids. Fig. 3 shows an image of such engineered foam. Most recently target improvements (full deuteration, advanced machining) resulted in an order of magnitude increase of DT and DD yields. We are currently awaiting an estimate of as-shot conditions, which we will then use to calculate a normalized ratio of the yield of the DT reactions to DD reactions – the key metric for comparison to theory.

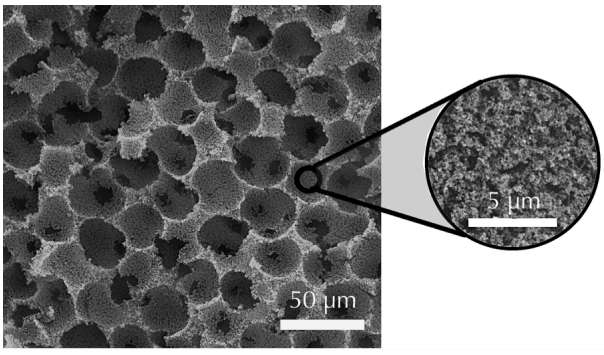

Figure 3: Marble CD foam with etched 30 micron voids.

Marble-VC

Marble is an experimental campaign intended to study the effects of heterogeneous mix on fusion burn. While designing the Marble implosion experiments, three questions emerged. First, how well do we understand the evolution of voids as the shock passes through? Is the evolution turbulent? Second, how well do we understand preheat inside our capsules, and finally, how accurate is the equation of state used for marble foams? To answer these questions, we designed an experimental campaign known as Marble Void Collapse. The idea was to take the well-understood shock-shear platform and modify it to answer these three questions. For the first type, a fine-cell 100 mg/cc CH foam filled the Rexolite tube as shown in figure 4 (a). Inside the foam, a sphere composed of iodine-doped CH foam (or tin-doped SiO_2 foam) was inserted. The density was chosen to be ~40 mg to give a similar Atwood number found in voids in the NIF foam capsules. The iodine (or tin) dopant was used to provide contrast with the Vanadium and Titanium backlighters. Figure (b) shows the second type, where a 6 µm thick aluminum foil was embedded inside shock tube to examine the expansion of the foil by preheat and measure the spread as the perturbed shock passed through the foil. The last type shown in figure (c), was filled with a marble CD foam where the void size was 50 µm in diameter. Throughout these three experiments, high quality radiographic data was acquired. The experimental result shown in figure (d) appears to confirm that the evolution of the void is not turbulent as the initial shock passes, seen in simulation. Also, the shock timing between simulation and experiment is well matched. This suggests accurate understanding of the fine-pore foam equation of state. As shown in figure (e), preheat effect was examined by the expansion of aluminum foil before a shock arrives. Figure (f) shows the shock speed measured thru marble foam (50 µm in diameter) and it can be used to determine the equation of state of the marble foam.

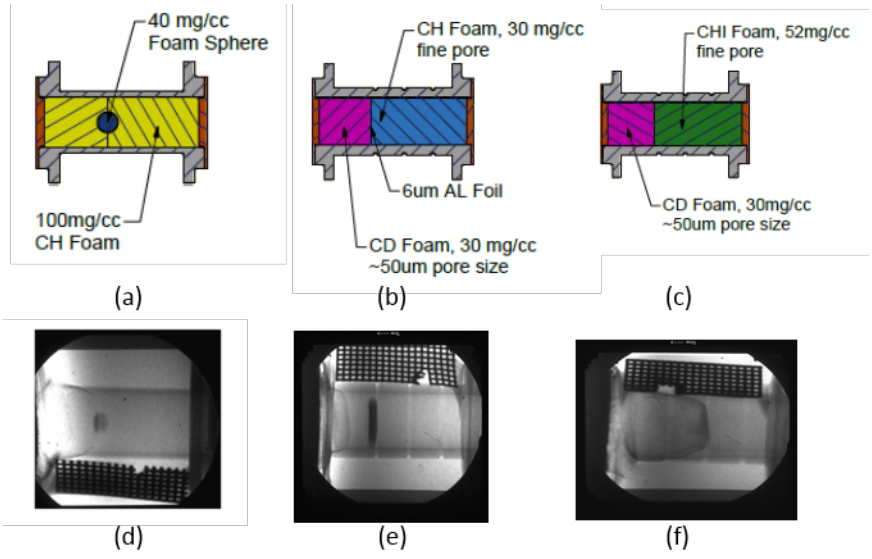

Figure 4: Three types of Marble Void Collapse setup (type a, b, and c). (d) evolution of void was not turbulent. (e) preheat effect was examined by the expansion of aluminum foil. (f) shock speed measured thru marble foam (50 µm in diameter) can be used to determine the equation of state of marble foam

CoaxDiff

The COAX experimental campaign on OMEGA develops an advanced radiation flow diagnostic useful for characterizing the subsonic and supersonic radiation front in order to provide constraining data for physics models. The intention is to eventually move these experiments to NIF. In these experiments, a halfraum is used to launch a radiation front down a cylindrical foam target (contained by a Be sleeve). The subsonic radiation front is measured through imaging, while spectroscopy of a doped insert in the target is utilized to study the supersonic form of the radiation front by observing its impact on the ionization balance of the dopant. Originally Ti was used, and was able to provide constraining data to the shape of the radiation front through comparison to PrismSPECT simulations. However, Ti K shell absorption spectra were unable to probe the shape of the front at temperatures below 100eV. In order to probe the potentially non-planckian character of the radiation front below 100eV, we elected to shift to a Sc dopant. Because Sc is lower Z than Ti, it requires less energy to exceed the ionization potential and therefore K-shell absorption spectra will occur at lower photon energies and lower temperatures than Ti. For both elements, absorption spectra are observed when photons generated by the laser-driven backlighter pass through the target and interact with electrons in autoionizing states in the L shell, enabling them to transition to a hole in the inner shell. At the current photon energy range of the NIF-5 spectrometer, Ti 1s-2p and Ti 1s-3p spectra are observable, but only Sc 1s-3p spectra are observable.

COAX had 3 shot days in FY16. In October 2015 imaging data and absorption spectra were observed for Ti and proof of principle was established for Sc by collecting Sc 1s-3p absorption spectra for the first time with the NIF-5. In April 2016 excellent image data of the doped aerogels were collected for both Ti and Sc doped foams, but issues with the spectroscopic backlighter resulted on only weak spectra being collected. In August a Kr-filled capsule backlighter design was successfully tested against a re-design of the previous wire backlighter, and a number of shots of strong Sc absorption spectra were collected using both backlighters. Initial data analysis suggests the T_e measured by the Sc was in the 75-90eV range. We did not collect imaging data in August, but instead used the space to collect constraining information about the size, brightness, and symmetry of the capsule backlighter, that is already beginning to inform the next set of experiments.

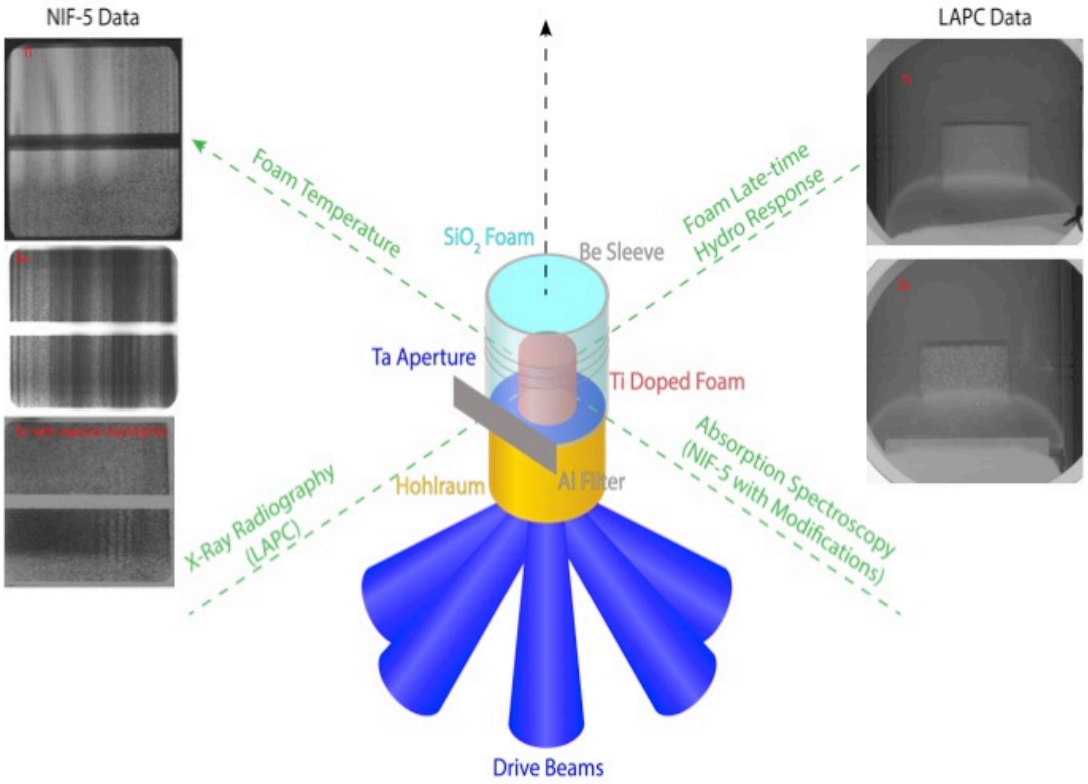

Figure 5: The target design is illustrated in a figure by J. Hager. On the left data collected for Ti from a prior year are compared to data from the latest shots with Sc in August. On the right, two radiographs from April with Sc and Ti doped aerogels are shown.

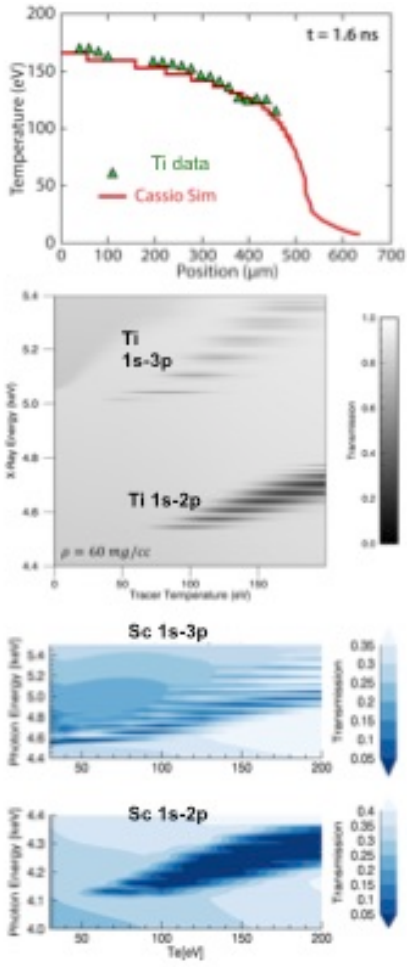

Figure 6: (Top) The shape of the radiation front in simulation is compared to results from COAX experiments featuring Ti-doped aerogels. Simulated K-shell absorption spectra from PrismSPECT for Ti (Center) and Sc (Bottom) illustrate the change in temperature and photon energy distribution of lines for the same transitions in two different elements. These figures were presented at the 2016 High Temperature Plasma Diagnostics Conference.

HEDmix

Anomalous low modes (particularly mode ~ 1) have been postulated as the cause of low hot-spot pressure of mid adiabat implosions in Omega direct drive [1,2]. In the 2016 HED-MIX campaign, images have captured emission signatures near stagnation, which are consistent with presence of such hypothesized low mode imbalance. The experiments used warm implosions with a Ti tracer at 1% by atom in the innermost 100 nm of the plastic shell. The Ti tracer emission was resolved spectrally using a unique imaging instrument termed the Multiple Monochromatic Imager (MMI) [3]. Fig. 7(a) shows an image obtained from 5-6 keV Ti emission at time of peak neutron production. A mode 1 pattern appears in the emission and is quantified (~70% drop) in Fig. 1(b). Such a pattern appeared

systematically within the day--though capsule mounting was excluded as the cause. Using 3-D modeling with LLE's ASTER code [2], we have found that such asymmetric emission results when such anomalous low modes are included in the drive. In the calculation, the emission drop results from reduced temperature on the over-driven side of the capsule where the tracer layer is compressed to higher density. To quantifiably estimate this density imbalance from the data, first the measured spectrum is modeled (see Fig. 7(c)) to determine the tracer conditions from the emissive region (n_e=5.75E24 cm^{-3}, T_e= 1350 eV). Beginning with these conditions, Fig. 7(d) shows the reduction in observed emission as density increases and temperature is decreased under assumption of pressure balance. Similar to the type of density modulations observed in the simulation, the results suggest about 50% variation in density of the emissive layer across the observed mode 1 pattern.

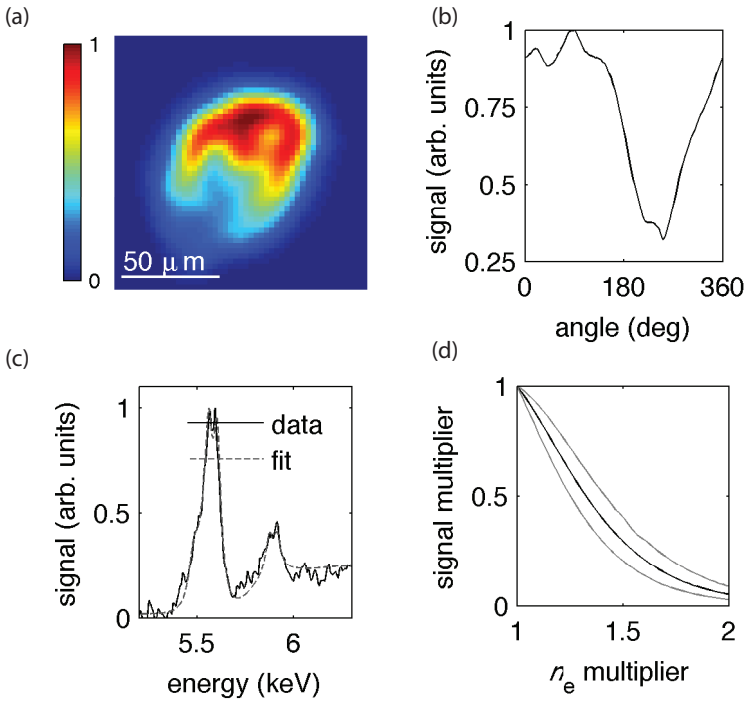

Figure 7: (a) Bang time image of Ti emission from 5-6 keV. (b) Peripheral signal versus angle. (c) Measured MMI spectrum and fit. (d) Modeled scaling of emission as density increases over nominal value from spectral fitting

[1] S. P. Regan *et al.* Phys. Rev. Lett. 117, 025001 (2016).

[2] I. V. Igumenshchev *et. al.* Phys. Plasmas 23, 052702 (2016).

[3] R. Tommasini *et. al.* Proc. of SPIE 6317, 631716 (2006).

HKMix

Mix is an important degradation mechanism for ICF, and there is a programmatic need for strong benchmarks for mix models. A new experimental platform has been developed, on this shot day and THDGamma-16A, to study mix. Differentially-thresholded GCDs measure the g-ray signal from a HT-fueled implosion with a deuterated shell, so that the HT burn comes from the core, while the DT reactions occur from any mix of shell material into the hot spot. The detector with lower gas pressure (higher threshold) is more sensitive to the HT-gs. On this experiment 860-µm diameter shells of 9 or 15µm thick plastic, with a 0.25µm thick inner deuterated layer, were filled with 9atm of equimolar HT gas. A simultaneous forward fit to the two detectors is then used to infer both DT and HT burn histories. The data from shot 80348, which used a 15µm thick shell, are shown in Fig. 8. The difference in time between the core and mix burn will be used to constrain time-dependent mix models. In this shot, the mix signal (DT) comes about 70ps later than the core (HT) burn. This result is corroborated by a second analysis technique that uses a surrogate shot without the deuterated layer, clearly showing the core (HT) signal comes early. The data from the 9µm-thick shells shows, in contrast, that the mix (DT) signal comes earlier than the core burn, suggesting the importance of a non-hydrodynamic mix process. This technique will be used over future campaigns by varying implosion parameters to study mix under various conditions.

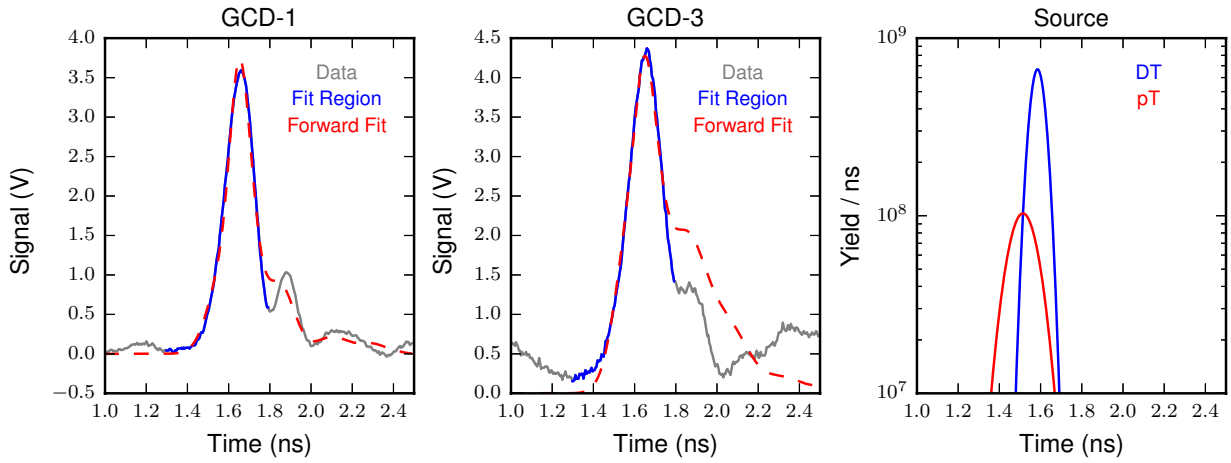

Fig 8: Cherenkov data from two detectors on shot 80348 using 100psi of CO2 (left) and 30psi of CO2 (center) on a mix shot. The data are simultaneously forward fit using burn histories for pT and DT reactions to infer the difference in time between the core (pT) and mix (DT) burn, shown at right.

MSP

Measuring charged-particle stopping power in dense plasmas relevant to ICF is challenging. The MSP-16A shot day tested a new technique based upon measuring charged-particle downshift in the compressed shell of an implosion. The target design is shown in Fig 9. A thick (25µm) CH shell is imploded with a fuel mixture of D/T/^{3}He. The DT-n inelastically scatter on the C in the shell, producing 4.4 MeV g rays that are detected with the GCDs, thus measuring the areal density of the shell at peak burn. Simultaneously, the 15 MeV D^{3}He protons are emitted and slow as they transit the shell. The

proton downshift gives a measurement of the average stopping power in the shell. A preliminary proton spectrum is shown in Fig 9, showing the proton downshift from their birth energy. X-ray spectroscopy (bottom right, Fig 9) was also used to characterize the plasma conditions in the shell, analyzing absorption lines produced by a 2% atomic Ti dopant in the shell. Analysis of the proton, x-ray, and g-ray data is continuing.

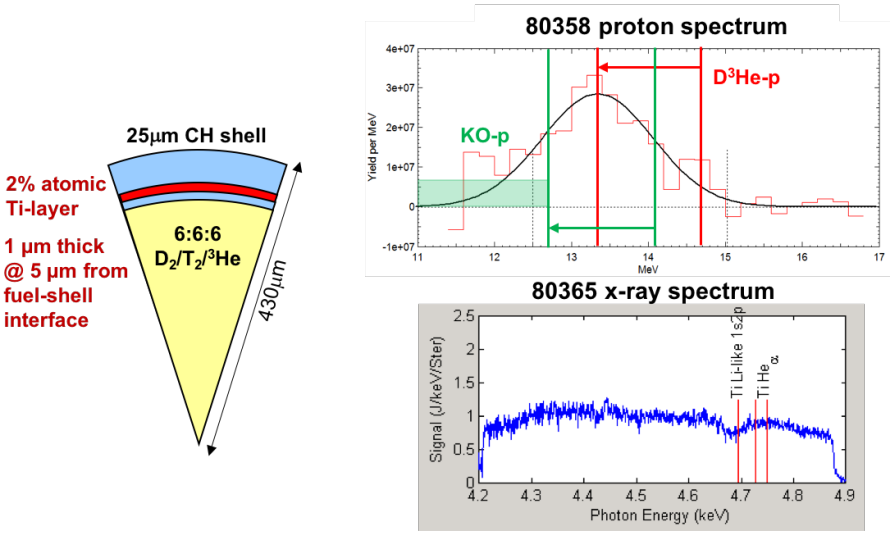

Figure 9: Target pie diagram (left). The D^3He proton spectrum measured on shot 80358 is shown at the top right, where the D^3He protons are downshifted from their birth energy by about 1.5 MeV. Knock-on (KO) protons are also observed, at lower energies, from elastic neutron scattering. The Ti-doped layer in the shell is used for absorption spectroscopy (bottom right) to diagnose the shell's plasma conditions.

ZSP

The ZSP-16A campaign studied charged-particle stopping power in warm-dense plasma. The experimental concept was based upon previous successful experiments in Be samples [1]. The experimental concept is shown in Fig. 10. The subject target is a 500μm thick graphite cylinder, doped with 1% atomic Pd, which is placed inside a Ti-coated tube. The tube is illuminated by 30 of the OMEGA laser beams, and the Ti x-ray emission isochorically heats the graphite sample. Au shield cones are placed on each end of the cylinder to shield the diagnostic line of sight from the laser spots. The sample is probed by protons or x rays along the TIM4-TIM6 axis.

Preliminary proton data from shot 80149 are shown at the right of Fig. 10. The proton source is a directly-driven exploding pusher, which creates an isotropic flux of 15 MeV D3He protons. The source spectrum is measured directly. The proton spectrum after transiting the graphite sample is also measured. The proton downshift is a direct measurement of the average stopping power in the sample. Additional proton data is being analyzed. X-ray absorption data from the Pd dopant will be analyzed to infer the plasma conditions.

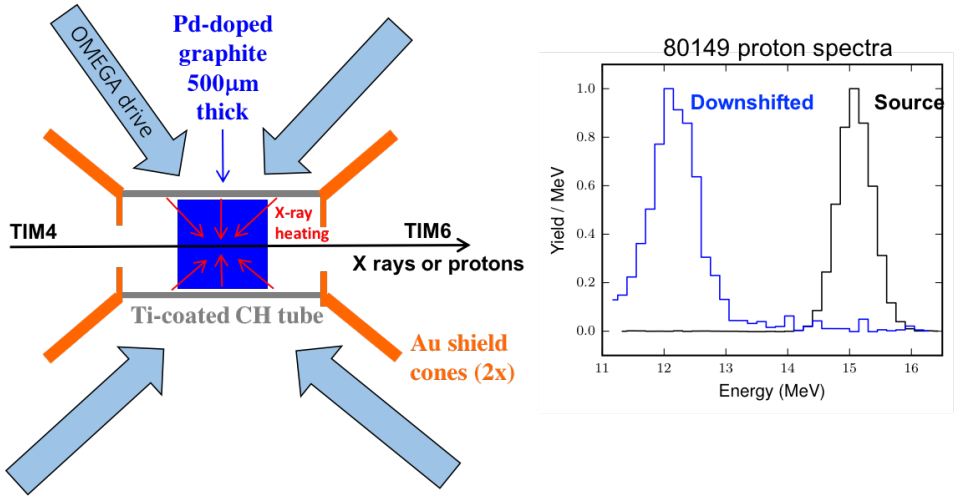

Figure 10: ZSP-16A experimental schematic (left) and proton spectrum (right). A cylindrical sample of Pd-doped graphite is heated isochorically by x rays generated at the outer surface of a Ti-coated tube. Probing protons or x rays sample the graphite along the axis. A sample proton spectrum from shot 80149 (peak normalized) is shown at right.

[1] A.B. Zylstra et al., Phys. Rev. Lett. 114, 215002 (2015)

THDGamma

The HT fusion reaction produces a mono-energetic gamma ray at 19.8 MeV. Thresholded Cherenkov detectors, like the GCDs [1], are relatively more sensitive to these higher-energy gammas than the DT-g (see Fig. 11a). The THDGamma-16A campaign was conducted to demonstrate the detection of HT-gammas and study the signals observed under different implosion conditions. 9 or 15 μm thick 860 μm diameter CH shells were filled with an equimolar mixture of H and T, with either 0.1% or 2.0% D contamination. The shots with 0.1% D, shown in Fig. 11b, show that the detector signal at 100psi of CO_2 is dominated by the HT- gs, as expected. This is the first definitive detection of these gamma rays produced from an ICF implosion. As the D concentration is increased, either in the initial gas fill or due to mix (e.g. from a CD shell), the relative importance of the DT- gamma contribution to the total signal increases. By using differentially-thresholded detectors, both reactions may be measured simultaneously. This technique will be used in an upcoming LANL mix campaign. Preliminary shots with deuterated shells were also taken on this day and used to iterate the implosion design for the subsequent experiments (HKMix-16A).

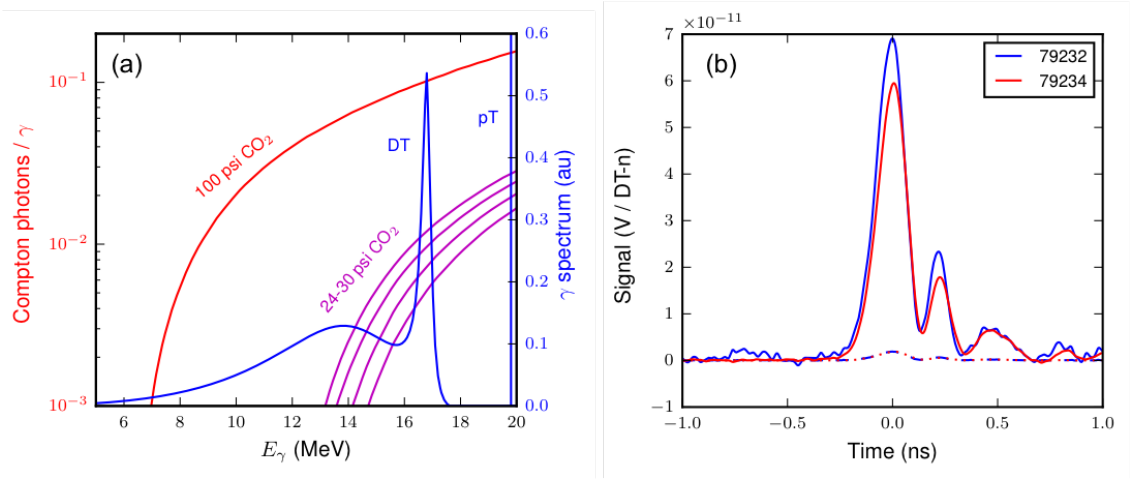

Figure 11: (a) Cherenkov detector response for various pressures of CO_2 gas compared to the g-ray spectrum from DT and HT fusion. The detector's relative sensitivity to HT g s increases for the lower gas pressures. (b) Signal from two H_2+T_2 fueled implosions, normalized to the DT-n yield. The GCD was fielded at 100psi CO_2. The dashed curves represent the signal contribution from DT-gs based on the measured DT-n yield, from a 0.1% D impurity. The signal is dominated by HT-gs, the first definitive detection of these g rays in ICF implosions.

[1] H.W. Herrmann et al., Rev. Sci. Instrum. 85, 11E124 (2014)

WDFEOS

The WDFEOS experiment collects information valuable for understanding the equation of state of warm dense matter under shocked conditions along the hugoniot. The WDM conditions explored are relevant for ICF and the interiors of Jovian planets. On the WDFEOS shot date in February 2016, low-density CH foams under shock compression in the 1-4Mbar range were studied using SOP and VISAR to measure shock velocity using shock breakout timing. After every VISAR/SOP shot there was an X-ray Thomson Scattering shot with the imaging x-ray Thomson spectrometer (iXTS) looking at scattering from the Ni He-a line at 7.8 keV, timed based on the shock breakout of the prior shot. Note in FIG. 12 the two types of targets have a different design to serve different purposes—the VISAR target includes a stepped foam to aid in the shock breakout measurement, while the IXTS target includes a thin Ni foil used to probe the shocked foam with 7.8-keV x-rays. The iXTS was used to primarily measure the temperature of the shocked foam.

Analysis of XRTS probe data thus far demonstrate that as the shock progresses through the foam in time there is a clear increase in T_e that appears as spectral broadening in the inelastic scattering feature. This also appears in time-integrated spectra within the same shots (i.e., the shock propagates down, and upper profiles are wider and hotter). This increase of T_e with time is indicative of preheat. Simulations including up 5 – 10eV of preheat show little change to final temperature but expansion in the preheated foam reduces the initial density and results in higher shock speeds. This estimate is in agreement with SOP and VISAR analysis that shows higher shock speeds than previous experiments.

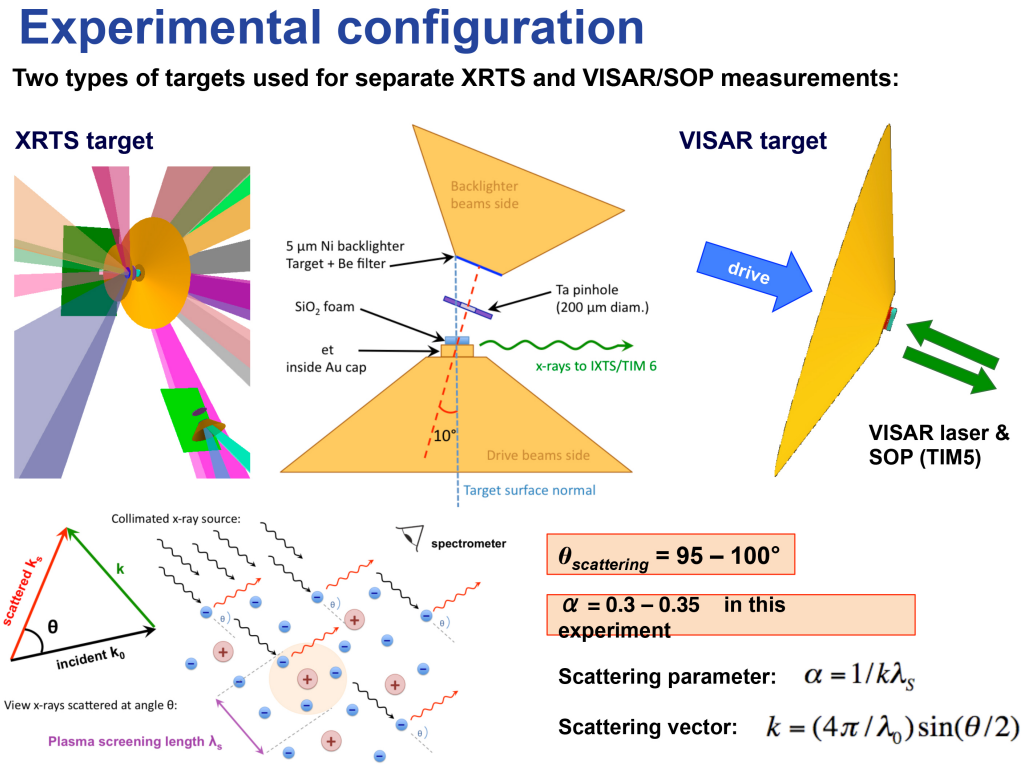

Figure 12: This figure includes schematics of the two types of targets used in WDFEOS experiments, as well as a simple explanation of the X-ray Thompson Scattering phenomenon.

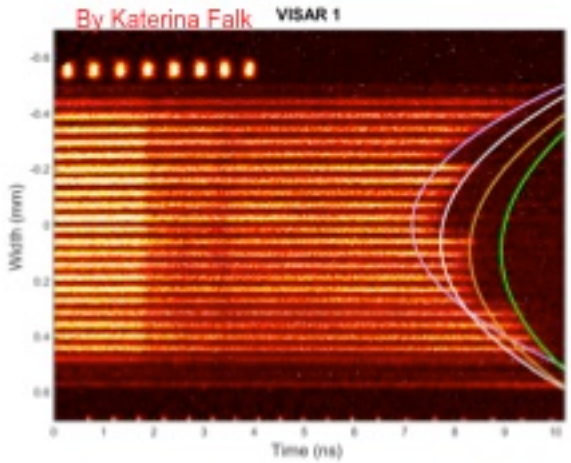

Figure 13: Parabolic fits to VISAR data, like the one shown, determine shock velocity based on shock breakout time. For Shot 80371, shock velocity is 82-95km/s at 5.5ns, 75-87km/s at 6.0ns, and 67-81km/s at 6.5ns.

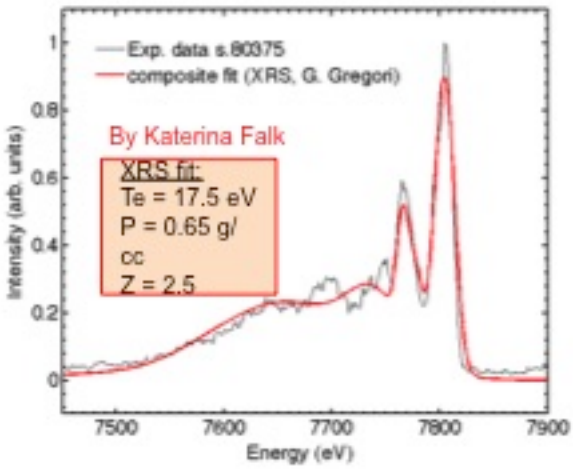

Figure 14: Temperature is determined by evaluating fits to the iXTS spectra after accounting for red-shift, contamination from blow-off plasma from the backlighter, and other corrections.

MixEOS-EP

Accurate simulations of fluid and plasma flows require accurate thermodynamic properties, which is typically represented by the equations of state (EOS) of the materials. For pure materials, the EOS may be represented by analytical models for idealized circumstances, or by tabular means, such as the Sesame tables. However, when a computational cell has a mixture of two or more fluids, the EOS is not well understood, particularly under the conditions of high energy densities. For these mixed cells, mixture rules are typically used to provide the requisite information; however, the accuracy of these rules is uncertain. We have conducted experiments at the OMEGA-EP laser facility providing EOS data, in the form of shock speed, of atomic mixtures of Ni and Al to study the mixed behavior and to validate various mixture rules used by our codes.

In our experiments we placed a quartz standard next to our test (NiAl) or reference (Al) metal specimen all on top of a thick ablator material used to efficiently create high pressure 10's Mbar shocks. This target geometry is shown in Fig. 15. With the ASBO we measured the shock velocity inside the quartz standard as well as the shock transit time through our opaque metal test specimens. Since the EOS of quartz is well-known, measuring the shock speed is sufficient to give us its shock pressure, which we also used to infer the shock pressure inside the ablator whose EOS we also assumed known (polystyrene and beryllium). Once the ablator shock pressure was known, along with any time dependent variations as measured inside the quartz, we could apply that pressure in our simulations for each mixture rule and see which gave the closest prediction to the measured shock transit time through the test specimen. We repeated the experiments on Al reference specimens, whose EOS is assumed known, to verify the strategy was sound.

In Fig. 16 we show the as-built target and raw ASBO streak camera data for a CH ablator/NiAl target (EP shot 22586) and a beryllium ablator/Al target (EP shot 22587). The ASBO viewed at the center of the target across the quartz/specimen interface extending about 400 μm on either side. In these data we observed the time at which the shock front broke out of the ablator and entered the quartz witness, the subsequent shock velocity history in the quartz witness, the time the shock broke out of the specimen, and the subsequent shock velocity in the quartz after leaving the specimen. We measured

shock velocities in our CH ablators of 43 km/s, which decreased to 35 km/s after entering the quartz due to differences in shock impedance at the interface. From shock transit time measurements we found a shock velocity of about 36 km/s in Al specimens and 31 km/s in NiAl. This NiAl shock speed most closely matches the mixture rules of "Additive Volume" and ideal gas mixing.

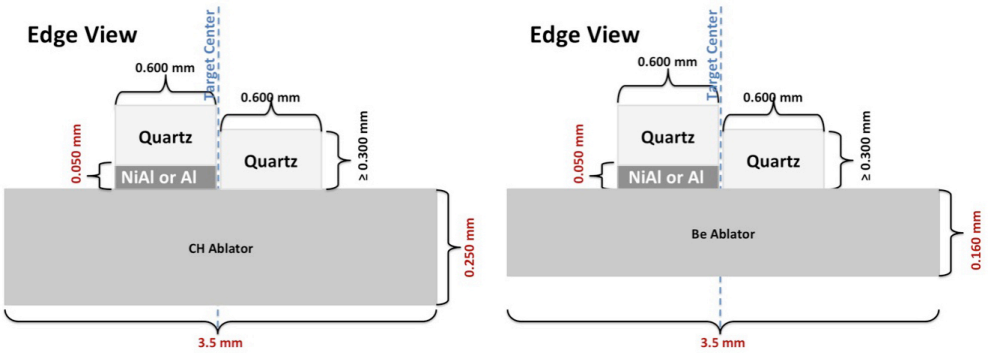

Figure 15: Illustration of the two types of MixEOS targets used where specimens and quartz reference windows were placed on top of thick ablators designed to create steady shocks without wave reverberations.

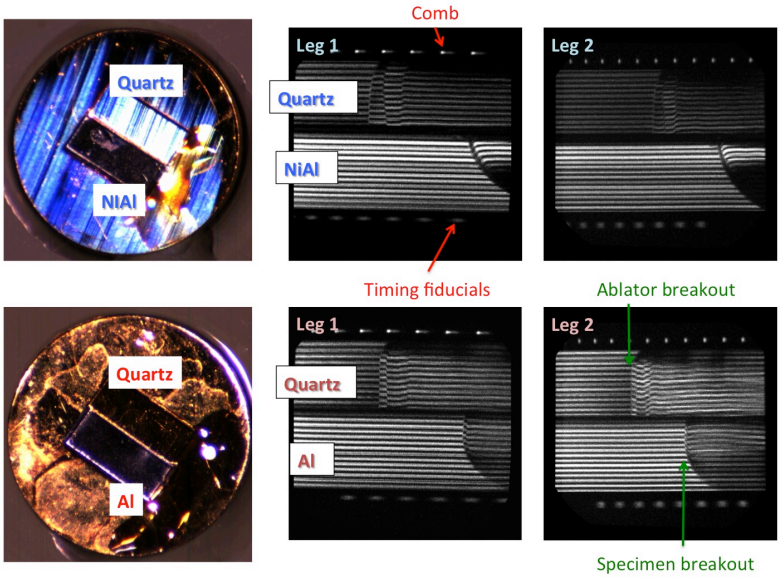

Figure 16: As-built targets and their ASBO streaked velocity data. Shock in the quartz is used to check steadiness and transit time through specimen gives specimen shock velocity.

ObliShock-EP

The mixing of modes between Rayleigh-Taylor (RT), Richtmeyer-Meshkov (RM) and Kelvin-Helmholtz (KH) instabilities occurs all across nature, from our terrestrial atmosphere and oceans [1] to

astrophyscial systems like accretion disks and supernovae [2]. The effects of shear on the growing spikes of the RT and RM processes is the reason for the production of the mushroom-like caps on these spikes [3], and can lead to a quicker onset and transition to turbulence [4]. Rarely is a flow interface purely shear or buoyancy driven; in the case of ICF, it is driven by a mix of passing shocks (RM), convergence (Bell-Plesset), and shearing shock flows (KH). The Oblique Shock platform developed by LANL in collaboration with the University of Michigan aims to understand the interplay between the various instabilities.

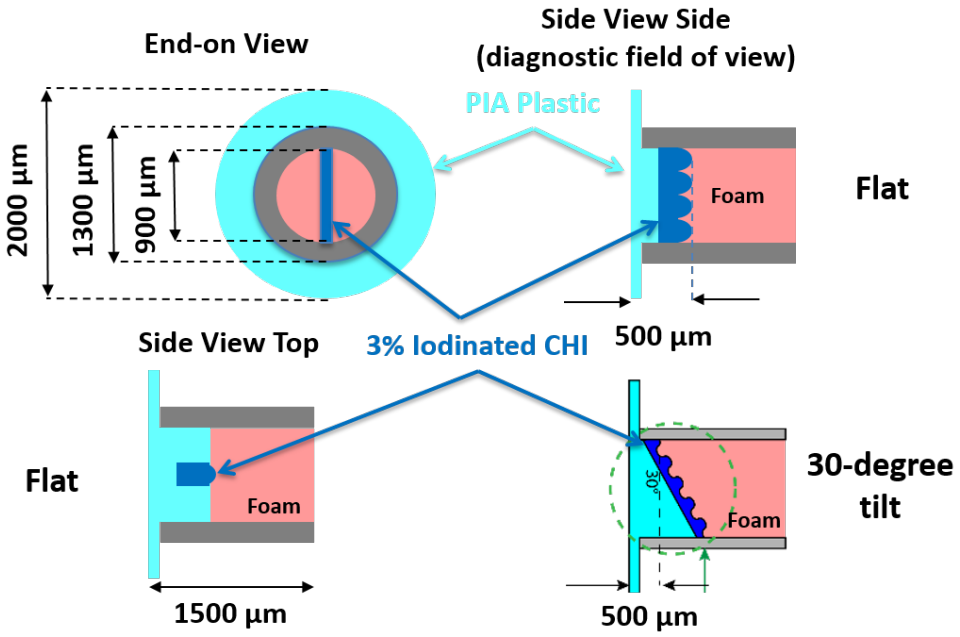

Figure 17. Setup of the Omega EP experiment. 3 long pulse 3-ω beams of ~5 kJ each simulataneously irradiate the PIA ablator top-hat (light-blue) and launch a shock into the experiment. A thin layer (100 microns) of density matched CHI (dark blue) is inserted into the PIA as a tracer layer for the perturbed interface inside a thin CH tube (grey). The tracer layer expands into a 100 mg/cc foam (red). A 0-degree tilt (upper right) and a 30-degree tilt (lower right) are illustrated. The interface evolution is then imaged at various times with the Spherical Crystal Imager (SCI) using an 8 keV copper K-α source driven by the 4th beam as a short-pule (10ps) backlighter. The area imaged by the SCI is indicated by the green dashed circle in the lower left 30-degree case. The field of view is shifted to follow the doped region as it transits the shock tube.

The platform, shown in Figure 17, is designed to allow one to control the amount of shear with respect to RM/RT growth. This is accomplished by a variable tilt interface. A steeper slope allows for more KH shear to enter the problem. Depicted is a 0-degree (upper right) and a 30-degree tilt (lower right) as seen by the diagnostic, the 30-degree case shows the field of view of the diagnostic (green dashed circle). The interface has an embedded strip of Iodinated CH (CHI) as a tracer layer for better imaging, and is density matched at ~1.45 g/cc to the surrounding polyimidamide (PIA) substrate (top-hat, light blue). When shocked using 3 of the EP beams at full power (~5 kJ) for 10 ns, the interface is pushed into a 100 mg/cc CH foam (Fig. 1 red) and is imaged using the Omega EP SCI from a short-pulse 10 ps Cu Kα backlighter onto image plates. The tracer layer is subject to several forces: shock

acceleration, deceleration into the foam, deceleration and decompression from the laser turn-off rarefaction, and shear flow across the layer, which cause a complex interplay of RM, RT, and KH in the growth of the spikes and bubbles seeded into the experiment. This is an important part of LANL's turbulent mix modeling strategy, including the implementation of a new modal model [5] coupled to the LANL BHR [6] mix model.

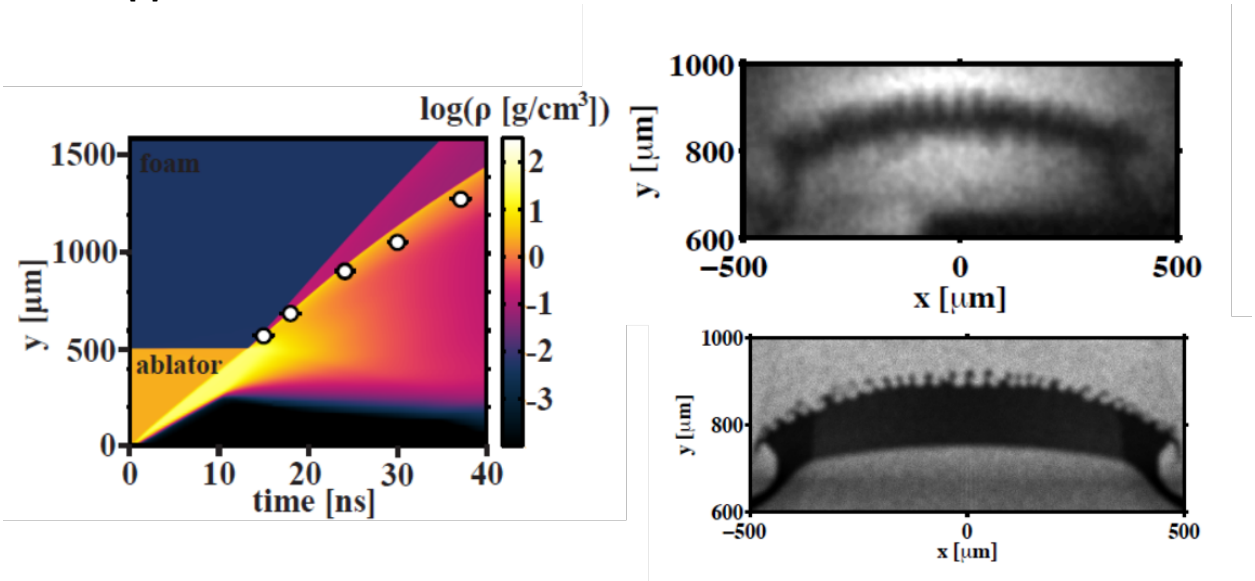

Figure 18. (left) Shock position/density jump as a function of time and (right) images of the multi-mode band experiment at 24 ns and a 2D RAGE simulation corresponding to the same time.

The first set of experiments were used to understand the shock velocity in the PAI/CHI and foam, to gauge our accuracy in modeling the platform the in the multi-physics code RAGE. The data from campaigns in FY15 was used to benchmark the platform [7]. Figure 18 shows the shock position from 1D RAGE simulations (left) next to one point in time from the experiment (top right) and the simulation (bottom left). The FY16 campaigns have been focusing on the observing mode coupling from multi-mode sine waves and a band of modes, to understand how the energy and growth is transferred from mode to mode[8]. The simulation shows similar growth of the layer and the characteristic turnover of the spikes due to the shear across the layer, but shows significantly more small-scale rollup than the experiment. The experiment is not well enough resolved to make out such small structures, but clearly exhibits the same rollup feature, which was expected due to the shear component in the system. The agreement is surprising considering the code used a simple mass-source as a pusher for the hydro-dynamics, which is unphysical at late time as the laser turns off at 10 ns and a rarefaction wave starts to enter the experiment, where in the code the source is on for the full simulation. This rarefaction catches up to the indicidual vortices at different times due to the varying ablator thickness, and vortex size can be seen to grow as the rarefaction catches up with each vortex. Work is currently ongoing to assess the growth rate of the spikes and bubbles using a new laser package for the RAGE calculations to simulate the full system end-to-end. This is the first step before using this data to help verify the modal model in a pure RT/RM configuration, i.e. 0-degrees.

1. W. R. Peltier and C. R. Caulfield, Annu. Rev. Fluid Mech. **35** (2003) 135 J.D. Woods, *J. Fluid Mech.* **32** (1968) 791

2. Lathrop, D.P. and C.B. Forest, "Magnetic dynamos in the lab." *Physics Today* **64**(7): 40-45 (2011); Xu, H., H. Li, D.C. Collins, S.T. Li, and M.L. Norman, "Turbulence and Dynamo in Galaxy Cluster Medium: Implications on the Origin of Cluster Magnetic Fields." *Astrophysical Journal Letters* **698**(1): L14-L17 (2009); Balbus, S.A. and J.F. Hawley, "Instability, turbulence, and enhanced transport in accretion disks." *Reviews of Modern Physics* **70**(1): 1-53 (1998); Bell, A.R., "Turbulent amplification of magnetic field and diffusive shock acceleration of cosmic rays." *Monthly Notices of the Royal Astronomical Society* **353**(2): 550-558 (2004); T. Ebisuzaki, T. Shigeyama, and K. Nomoto, *Astrophys. J.* 344, L65 (1989); I. Hachisu, T. Matsuda, K. Nomoto, and T. Shigeyama, *Astrophys. J.* 358, L57 (1990).
3. T. Yabe, H. Hoshino, and T. Tsuchiya, Two- and three-dimensional behavior of Rayleigh–Taylor and Kelvin-Helmholtz instabilities, Phys. Rev. A, 44, (1991) 2756 and N. J. Zabusky, Annu. Rev. Fluid Mech. 31, (1999) 495
4. Y. Zhou, B. A. Remington, H. F. Robey, A. W. Cook, S. G. Glendinning, A. Dimits, A. C. Buckingham, G. B. Zimmerman, E. W. Burke, T. A. Peyser, W. Cabot, and D. Eliason, Phys. Plasmas, 10, (2003) 1883 and Y.Zhou, H.F. Robey, and A.C. Buckingham, Phys. Rev. E , 67 (2003) 056305 and Y. Zhou, Phys. Plasmas, 14 (2007) 082701
5. B. Rollin and M. J. Andrews, *J. Turb.* **14**, 77-106 (2013)
6. D. Besnard, F. Harlow, and R. Rauenzahn, Conservation and transport properties of turbulence with large density variations, Tech. Rep. LA-10911-MS (Los Alamos National Laboratory, 1987).
7. G. Malamud, et al. *HEDP* **9**, 122-131 (2013)
8. C. A. Di Stefano, A. M Rasmus, F. W. Doss, K. A. Flippo, J. D. Hager, and J. L. Kline, *Appl. Phys. Lett.* (submitted)
9. A. M. Rasmus, C. A. Di Stefano, F. W. Doss, K. A. Flippo, and J. L. Kline, *Phys. Rev. Lett.* (in preparation)